IEEE Access
Multidisciplinary | Rapid Review | Open Access Journal

Received February 25, 2019, accepted March 4, 2019, date of publication March 8, 2019, date of current version April 2, 2019.

Digital Object Identifier 10.1109/ACCESS.2019.2903831

A 3D Wireless Charging Cylinder With Stable Rotating Magnetic Field for Multi-Load Application

HUA HAN[1,2], ZHU MAO[1,2], QI ZHU[1,2], (Student Member, IEEE), MEI SU[1,2], AND AIGUO PATRICK HU[3], (Senior Member, IEEE)

[1]School of Automation, Central South University, Changsha 410083, China
[2]Hunan Provincial Key Laboratory of Power Electronics Equipment and Grid, Changsha 410083, China
[3]Department of Electrical and Computer Engineering, The University of Auckland, Auckland 1023, New Zealand

Corresponding author: Qi Zhu (csu_zhuqi@163.com)

This work was supported in part by the National Natural Science Foundation of China under Grant 61573384, in part by the Project of Innovation-Driven Plan in Central South University under Grant 2019CX003, in part by the National Key R&D Program of China under Grant 2018YFB0606005, in part by the Fundamental Research Funds for the Central Universities of Central South University under Grant 2018zzts525, and in part by the Scholarship from the China Scholarship Council under Grant 201706370068.

ABSTRACT This paper proposes a 3D wireless charging cylinder with improved compensation topology to generate a stable rotating magnetic field for charging multiple loads around it. The induced voltage of each receiver is kept constant against load variations when the distance between the transmitter and the receiver is fixed. The 3D charging cylinder has a simple configuration with two perpendicular LCL-compensated transmitter coils driven by separate power inverters sharing a common dc source. The system is fully analyzed with the maximum load limit determined, and design guidance is provided. Both theoretical and experimental results demonstrate that the transmitter currents remain constant against load variations when the total load is within the maximum load limit, and the transfer efficiency is increased with the increase of the total reflected impedance. Compared to the conventional series–series (SS) compensated WPT system, the proposed 3D configuration can maintain the transmitter currents to be constant within the maximum load limit so that multiple loads can be added without affecting each other. It has found that the transmitter currents of the proposed configuration are kept constant at their initial values when four loads with the resistance of 0.5 Ω each are randomly placed at 21 cm from the center of the charging cylinder. By contrast, the transmitter currents of the SS compensated WPT system are obviously changed together with the load voltages.

INDEX TERMS 3D wireless charging cylinder, constant induced voltage, maximum load limit, multi-load application, stable rotating magnetic field.

I. INTRODUCTION

Wireless power transfer (WPT) has been an emerging technology because of its convenience, simplicity and safety. During the last two decades, the WPT technology has made rapid progress covering smart phone, wearable device, medical equipment, transportation and other fields [1]–[7]. In the conventional studies, transfer efficiency and distance are two issues that researchers are most concerned about. Lots of methods are proposed to improve the performance of the WPT system, such as designing coil structure [8], [9], choosing proper compensation network [10], [11], introducing magnetic resonant coupling [12], [13], adding repeaters [14], [15], etc. However, these studies usually focus on the planar WPT system which has low degree of freedom (DOF).

In order to expand the DOF of WPT system, one solution is to shape the resultant magnetic field generated by multi-phase transmitter coils through controlling the currents of the transmitter coils. O'Brien [16] proposed the method of using orthogonal coils for omnidirectional WPT system. Lin et al. [17] provided the basic mathematical theory of two-dimensional (2D) omnidirectional WPT system. Lim and Park [18] introduced beamforming theory into 2D WPT system and proposed a phase-control-based method which

The associate editor coordinating the review of this manuscript and approving it for publication was Huiqing Wen.

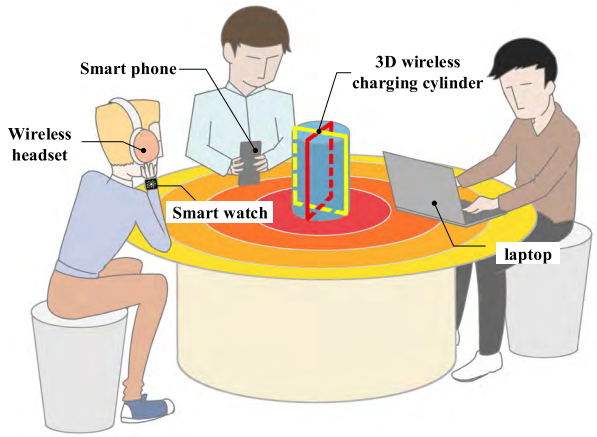

FIGURE 1. Application of the proposed 3D wireless charging cylinder.

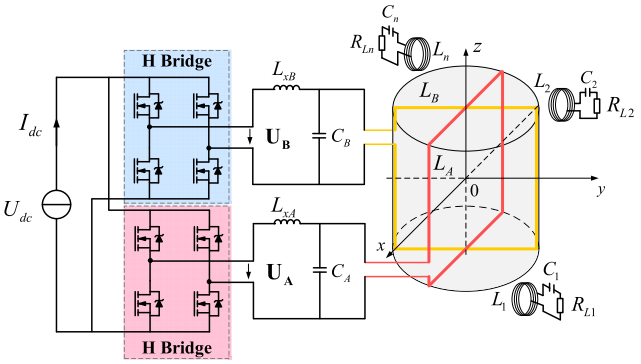

FIGURE 2. 3D wireless charging cylinder with multi-load.

formed magnetic field in particular directions. To further increase the DOF in space, Zhu et al. [19] extended this theory to three-dimensional (3D) WPT system, and realized 3D full-range field orientation with adjustable magnitude and direction of B-field at an arbitrary point. However, the above studies are dedicated to concentrate the resultant magnetic field to a certain direction. Another way is to produce a rotating magnetic field. Mei et al. [20] investigated a two-phase WPT system consisting of two orthogonal transmitter coils, which generated the rotational magnetic field by employing a phase-shift angle control method. Raval et al. [21] proposed a 3D inductive power system driven by a multiple-phase power converter, which produced a rotating magnetic field by generating phase quadrature currents.

With a rotating magnetic field obtained, charging only one load cannot achieve the maximum utilization of energy. It is desired to charge multi-load simultaneously with high DOF and stable performance, such as providing stable charging voltage, unaffected for load variations, no controller required and without communication link.

This paper proposes a 3D wireless charging cylinder for multi-load application. As is shown in Fig. 1, the 3D wireless charging cylinder set on the center of the table provides a rotating magnetic field. Controller and communication link are eliminated in this system and the magnetic field generated by the transmitters is unaffected by load variations within the maximum load limit. Mobile devices placed on arbitrary position around the cylinder are able to receive stable charging voltage. This paper studies one simple system configuration, which meets all the above demands, but in practice, it is not just limited to this solution. In this system, two LCL-compensated transmitter coils are used and placed perpendicular to each other. The receiver adopts series compensation topology, which ensures the consistency of load voltage and induced voltage. For ease of analysis, the receiver coil is perpendicular to the direction of magnetic field. In order to analyze the system comprehensively, the output performance and transfer efficiency with load variations are studied including the number of loads, the impedance of loads and the distance between the transmitter and loads. The maximum load limit of keeping stable rotating magnetic field is analyzed and the system parameters design guidance is concluded. Finally, a system performance comparison between the proposed configuration and the conventional series-series (SS) WPT system is discussed.

The rest of this paper is organized as follows: The system configuration and mathematical model of 3D wireless charging cylinder used in this paper is introduced in section II. In section III, the system is theoretical analyzed, design guidance of the system parameters is given. In section IV, a 3D-hardware system is established, and the experimental results validate the effectiveness of the proposed system configuration. Finally, a conclusion is drawn in section V.

II. PROPOSED 3D WIRELESS CHARGING CYLINDER

A. SYSTEM CONFIGURATION AND OPERATING PRINCIPLE

As can be seen from Fig. 2, U_{dc} is the DC voltage source utilized in this WPT system and I_{dc} is the DC input current. Two H-bridge inverters are independently controlled to convert the DC voltage into two AC sinusoidal voltage sources, marked as $\mathbf{U_A}$ and $\mathbf{U_B}$. L_A and L_B are two transmitter coils. The transmitter coil is first connected in parallel with resonant capacitors (C_A or C_B) and then in series with additional inductors (L_{xA} or L_{xB}), which constitutes the LCL circuit of each transmitter. L_i ($i = 1, 2, \ldots, n$) is the receiver coil and is connected in series with capacitor C_i and load R_{Li}. The two transmitter coils are perpendicular to each other, so that the coupling factor between them is ignored theoretically. The transmitter coils are covered by an outer covering, whose material has no effect on the distribution of the spatial magnetic field. In the rest of the paper, the outer covering is not shown for clear observation. Compared with the mutual inductance between the transmitter coils and the receiver coils, the mutual inductances between each two receiver coils are tiny, they are not considered for simplifying the subsequent analysis.

To achieve the multi-load simultaneously charged, the high-frequency rotating magnetic field is generated, and the phase-shift control is utilized. The phasor expressions of two

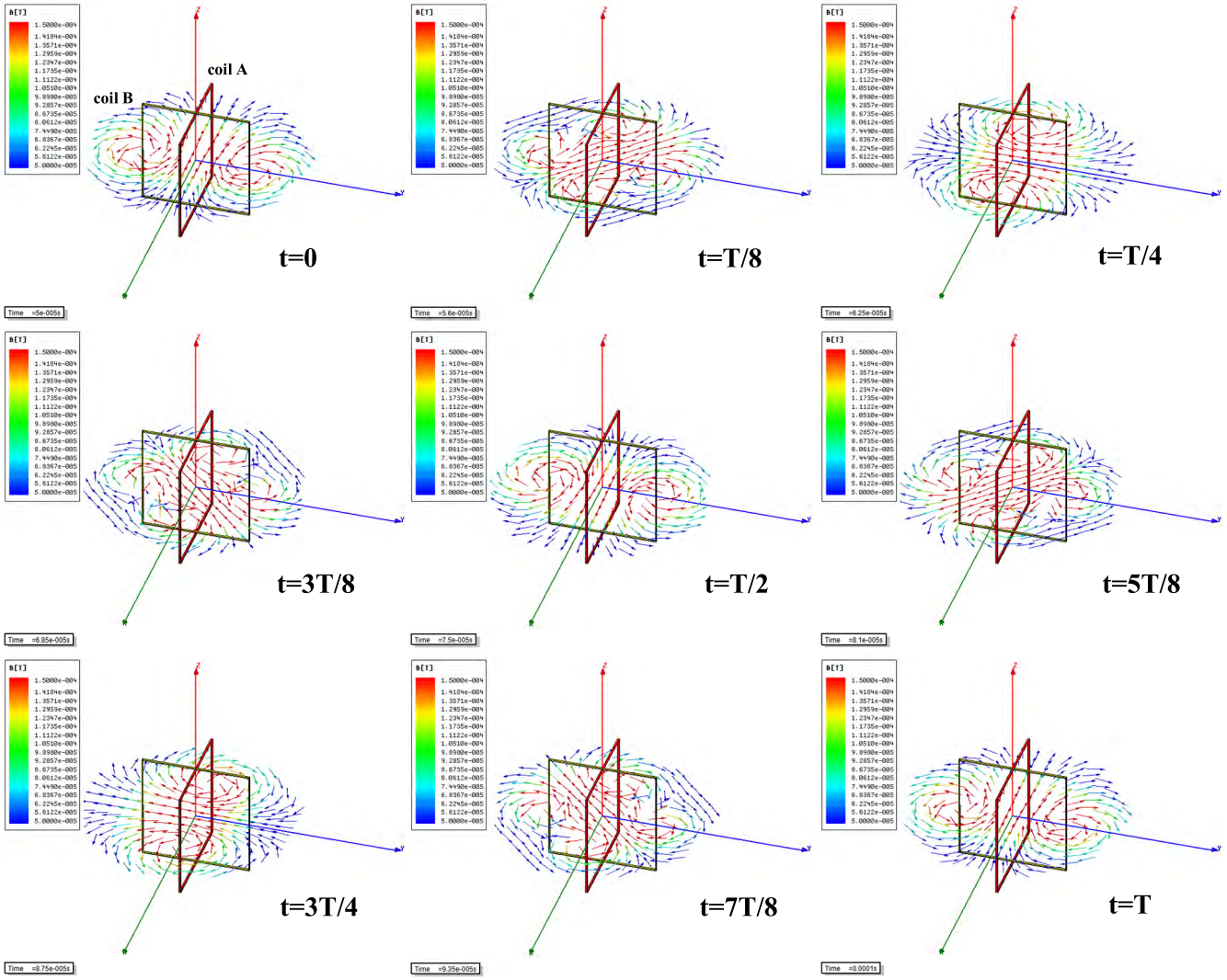

FIGURE 3. Variation of the magnetic field distribution during one period.

transmitter currents are given as:

$$\mathbf{I_A} = I\angle 0^\circ \tag{1}$$

$$\mathbf{I_B} = I\angle \theta \tag{2}$$

where I represents the effective value of two transmitter currents, θ represents the phase-shift angle of two transmitter currents. The resultant magnetic field vector rotates in a full circle and covers all the directions of *xoy* plane when θ is set around 90° [20]. In this paper, θ is set to 90°. With the help of Ansoft Maxwell, the simulated B-field during one period T is displayed in Fig. 3 and the parameters are given in Table 1.

When the resultant magnetic field vector rotates at high-frequency, the rotation period of magnetic field is much smaller than the time constant of RLC circuit of the receiver. It is reasonable that multiple loads are simultaneously charged when they are placed in the charging area.

TABLE 1. Simulation parameters of the proposed 3d wireless charging cylinder.

Description	*Parameter*	*Value*
Operating frequency	f	20kHz
Inductance of transmitter coils	L_A, L_B	10 μH
Resonant capacitor	C_A, C_B	6.33 μF
Additional inductor of transmitters	L_{xA}, L_{xB}	10 μH
Side length of transmitter coils	l	300mm
Turns of transmitter coils	N	3
Wire radius of transmitter coils	r	2.2mm

B. MATHEMATICAL MODEL OF THE 3D WIRELESS CHARGING CYLINDER

Assuming that there are two loads around the 3D wireless charging cylinder, the equivalent circuit model of this WPT system is shown in Fig. 4. R_{xA} and R_{xB}, R_A and R_B

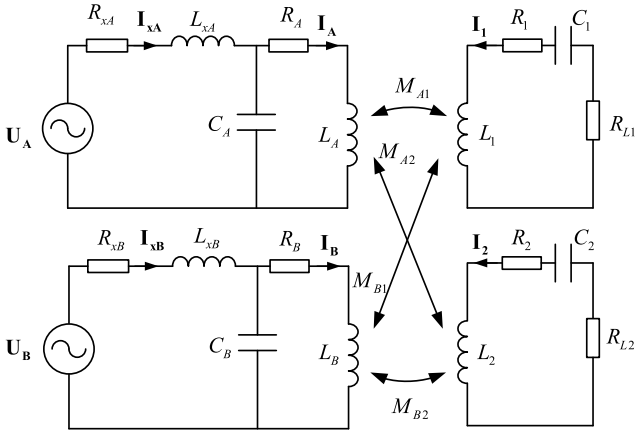

FIGURE 4. Equivalent circuit model of the proposed WPT system with two loads.

are the parasitic resistors of additional inductors, transmitter coils, respectively. M_{Ai} and M_{Bi} represent mutual inductance between the transmitter coil (coil A or coil B) and the receiver coil $i(i = 1, 2)$. According to Kirchhoff's voltage law, the model of receiver is expressed as:

$$\begin{bmatrix} 0 \\ 0 \end{bmatrix} = \begin{bmatrix} -j\omega M_{A1} & -j\omega M_{B1} & Z_1 & 0 \\ -j\omega M_{A2} & -j\omega M_{B2} & 0 & Z_2 \end{bmatrix} \begin{bmatrix} \mathbf{I_A} \\ \mathbf{I_B} \\ \mathbf{I_1} \\ \mathbf{I_2} \end{bmatrix} \tag{3}$$

where,

$$Z_i = j\omega L_i + \frac{1}{j\omega C_i} + R_i + R_{Li} \tag{4}$$

where $Z_i(i = 1, 2)$ is the total impedance of the i^{th} receiver.

R_i and R_{Li} represent the parasitic resistance and load resistance of the i^{th} receiver. Taking the transmitter A as an example, when two receivers are reflected to the transmitter, the equivalent circuit of the transmitter A is illustrated in Fig. 5. The reflected impedance of load 1 and load 2 are denoted as Z_{rAi} $(i = 1, 2)$. Combining (1-3) Z_{rAi} is expressed as follows.

$$Z_{rAi} = \frac{\omega^2 M_{Ai}^2 + \omega^2 M_{Ai} M_{Bi} \frac{\mathbf{I_B}}{\mathbf{I_A}}}{Z_i} = \frac{\omega^2 M_{Ai}^2 + j\omega^2 M_{Ai} M_{Bi}}{Z_i} \tag{5}$$

Then the transmitter A can be mathematical expressed as:

$$\mathbf{U_A} = \mathbf{I_{xA}} Z_A \tag{6}$$

where $\mathbf{I_{xA}}$ is the current through the additional inductor L_{xA} in Fig. 5 and Z_A is the total equivalent impedance of the transmitter A, and

$$Z_A = R_{xA} + j\omega L_{xA} + \frac{1}{j\omega C_A} // (R_A + j\omega L_A + \sum_{i=1}^{2} Z_{rAi}) \tag{7}$$

The transmitter current $\mathbf{I_A}$ is calculated as:

$$\mathbf{I_A} = \mathbf{I_{xA}} \cdot \frac{\frac{1}{j\omega C_A}}{\frac{1}{j\omega C_A} + R_A + j\omega L_A + \sum_{i=1}^{2} Z_{rAi}} \tag{8}$$

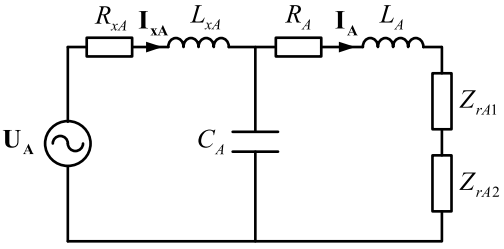

FIGURE 5. Equivalent circuit of the transmitter A.

Similarly, the equivalent circuit of the transmitter B can be mathematical expressed as:

$$\mathbf{U_B} = \mathbf{I_{xB}} Z_B \tag{9}$$

where,

$$Z_B = R_{xB} + j\omega L_{xB} + \frac{1}{j\omega C_B} // (R_B + j\omega L_B + \sum_{i=1}^{2} Z_{rBi}) \tag{10}$$

$$Z_{rBi} = \frac{\omega^2 M_{Bi}^2 + \omega^2 M_{Ai} M_{Bi} \frac{\mathbf{I_A}}{\mathbf{I_B}}}{Z_i} = \frac{\omega^2 M_{Bi}^2 - j\omega^2 M_{Ai} M_{Bi}}{Z_i} \tag{11}$$

$\mathbf{I_{xB}}$ is the current through the additional inductor L_{xB}, Z_B is the total equivalent impedance of the transmitter B, and $Z_{rBi}(i = 1, 2)$ represents the reflected impedance of load 1 and load 2 in the transmitter B.

The transmitter current $\mathbf{I_B}$ can be calculated as:

$$\mathbf{I_B} = \mathbf{I_{xB}} \cdot \frac{\frac{1}{j\omega C_B}}{\frac{1}{j\omega C_B} + R_B + j\omega L_B + \sum_{i=1}^{2} Z_{rBi}} \tag{12}$$

III. SYSTEM THEORETICAL ANALYSIS

A. TRANSMITER CURRENT AND INDUCED VOLTAGE

When the WPT system operates at the resonant frequency, each inductor and its corresponding capacitor resonate at the operating frequency, where $\omega^2 L_A C_A = 1$, $\omega^2 L_1 C_1 = 1$ and $\omega^2 L_2 C_2 = 1$. Compared with their inductances, the parasitic resistances are tiny and ignored, then the impedance Z_A is simplified as:

$$Z_A = j\omega L_{xA} + \frac{1}{j\omega C_A} + \frac{L_A}{C_A(Z_{rA1} + Z_{rA2})} \tag{13}$$

Based on (6), (8), (13), the transmitter current $\mathbf{I_A}$ is deduced as:

$$\mathbf{I_A} = \frac{\mathbf{U_A}}{j(\omega L_{xA} - \frac{1}{\omega C_A}) + \frac{L_A}{C_A(Z_{rA1}+Z_{rA2})}} \cdot \frac{1}{j\omega C_A(Z_{rA1} + Z_{rA2})} \tag{14}$$

Under the condition of $L_{xA} = L_A$, which means $\omega^2 L_{xA} C_A = 1$, $\mathbf{I_A}$ can be further simplified as:

$$\mathbf{I_A} = \frac{\mathbf{U_A}}{j\omega L_A} \tag{15}$$

The expression of the transmitter current $\mathbf{I_B}$ is derived in the same way and displayed as:

$$\mathbf{I_B} = \frac{\mathbf{U_B}}{j\omega L_B} \tag{16}$$

According to (15) and (16), the transmitter current is determined only by the AC supply voltage and the inductance of the transmitter coil itself when parasitic resistors are ignored. The variation of loads will not affect the transmitter currents. Under the full resonance, the induced voltage of the i^{th} receiver and the corresponding output voltage can be expressed as:

$$\mathbf{U}_i = j\omega M_{Ai}\mathbf{I_A} + j\omega M_{Bi}\mathbf{I_B} \tag{17}$$

$$\mathbf{U}_{Li} = \mathbf{U}_i \cdot \frac{R_{Li}}{R_{Li} + R_i} \tag{18}$$

In practical applications, the parasitic resistor R_i of the i^{th} receiver coil is usually much smaller than the load resistance R_{Li}, consequently, the output voltage equals to the induced voltage. It can be inferred from (17-18) that the induced voltage and output voltage keeps constant once the load position is fixed.

B. OUTPUT POWER AND TRANSFER EFFICIENCY

1) INDIVIDUAL LOAD

Assuming the number of loads placed in the charging area is n. According to equation (1-3), the current flowing through the load i can be calculated as follows.

$$\mathbf{I}_i = \frac{j\omega M_{Ai}\mathbf{I_A} + j\omega M_{Bi}\mathbf{I_B}}{Z_i} = \frac{j\omega M_{Ai} I - \omega M_{Bi} I}{R_i + R_{Li}} \tag{19}$$

The effective value of load current is:

$$||\mathbf{I}_i|| = \frac{\sqrt{(\omega M_{Ai})^2 + (\omega M_{Bi})^2}}{R_i + R_{Li}} \cdot I \tag{20}$$

Then the delivered power P_{rei} and output power P_{Li} of the i^{th} receiver can be calculated as:

$$P_{rei} = ||\mathbf{I}_i||^2 Re(Z_i) = \frac{(\omega M_{Ai})^2 + (\omega M_{Bi})^2}{R_i + R_{Li}} \cdot I^2 \tag{21}$$

$$P_{Li} = P_{re} \cdot \frac{R_{Li}}{R_i + R_{Li}} = \frac{(\omega M_{Ai})^2 + (\omega M_{Bi})^2}{(R_i + R_{Li})^2} \cdot I^2 R_{Li} \tag{22}$$

In order to analyze the transfer performance of the system, only the transfer efficiency from equivalent AC sources to load power is considered. To find out the total consumed power from two AC sources, power loss on parasitic resistance of all inductors should be considered. As shown in Fig. 5, the total consumed power of $\mathbf{U_A}$ can be expressed as:

$$P_A = ||\mathbf{I_{xA}}||^2 Re(Z_A) \tag{23}$$

where $||\mathbf{I_{xA}}||$ is effective value of the main street current and $Re(Z_A)$ is the real part of total equivalent impedance. Based on (7-8), $||\mathbf{I_{xA}}||$ and $Re(Z_A)$ are calculated as:

$$||\mathbf{I_{xA}}|| = ||\mathbf{I_A} \cdot j\omega C_A (R_A + \sum_{i=1}^{n} Z_{rAi})|| = I \cdot \omega C_A \sqrt{(R_A + \sum_{i=1}^{n} \frac{\omega^2 M_{Ai}^2}{R_i + R_{Li}})^2 + (\sum_{i=1}^{n} \frac{\omega^2 M_{Ai} M_{Bi}}{R_i + R_{Li}})^2} \tag{24}$$

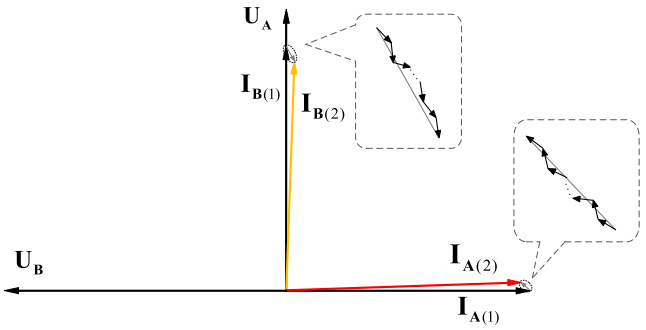

FIGURE 6. Variation of two transmitter currents.

TABLE 2. Actual circuit parameters of transmitters.

Description	*Parameter*	*Value*
DC voltage source	U_{dc}	27V
Operating frequency	f	20kHz
Inductance of transmitter coil A(red)	L_A	10.06 μH
Inductance of transmitter coil B(yellow)	L_B	10.09 μH
Parasitic resistance of transmitter coil A	R_A	50.23m Ω
Parasitic resistance of transmitter coil B	R_B	50.30m Ω
Resonant capacitor of Coil A	C_A	6.61 μF
Resonant capacitor of Coil B	C_B	6.59 μF
Additional inductor of transmitter A	L_{xA}	9.60 μH
Additional inductor of transmitter B	L_{xB}	9.67 μH
Parasitic resistance of additional inductors	R_{xA} , R_{xB}	2.4m Ω
Side length of transmitter coil A, B	l	328mm

$$Re(Z_A) = Re(R_{xA} + \frac{L_A}{C_A(R_A + \sum_{i=1}^{n} Z_{rAi})}) = R_{xA} + \frac{L_A C_A (R_A + \sum_{i=1}^{n} \frac{\omega^2 M_{Ai}^2}{R_i + R_{Li}})}{C_A^2 [(R_A + \sum_{i=1}^{n} \frac{\omega^2 M_{Ai}^2}{R_i + R_{Li}})^2 + (\sum_{i=1}^{n} \frac{\omega^2 M_{Ai} M_{Bi}}{R_i + R_{Li}})^2]} \tag{25}$$

Similar to the transmitter A, the total consumed power of $\mathbf{U_B}$ can be obtained.

$$P_B = ||\mathbf{I_{xB}}||^2 Re(Z_B) \tag{26}$$

where $||\mathbf{I_{xB}}||$ is effective value of the main street current and $\text{Re}(Z_B)$ is the real part of total equivalent impedance. Based on (10-12), $||\mathbf{I_{xB}}||$ and $\text{Re}(Z_B)$ are calculated as:

$$||\mathbf{I_{xB}}|| = ||\mathbf{I_B} \cdot j\omega C_B (R_B + \sum_{i=1}^{n} Z_{rBi})|| = I \cdot \omega C_B \sqrt{(R_B + \sum_{i=1}^{n} \frac{\omega^2 M_{Bi}^2}{R_i + R_{Li}})^2 + (\sum_{i=1}^{n} \frac{\omega^2 M_{Ai} M_{Bi}}{R_i + R_{Li}})^2} \tag{27}$$

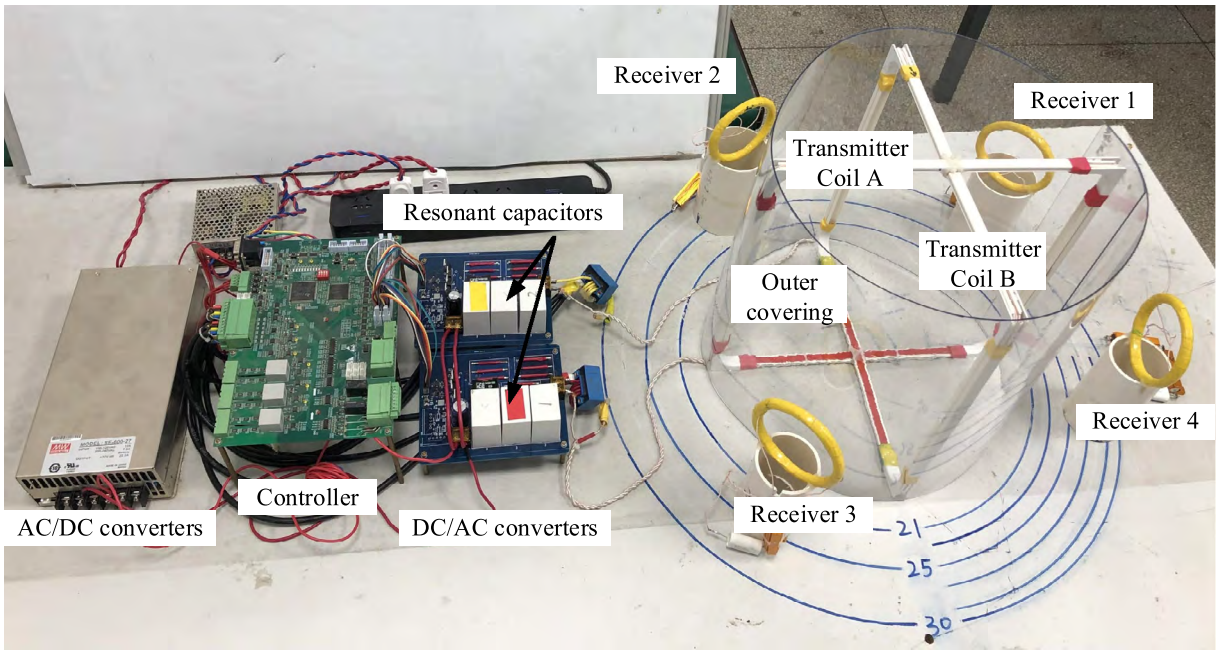

FIGURE 7. Proposed WPT system experimental platform.

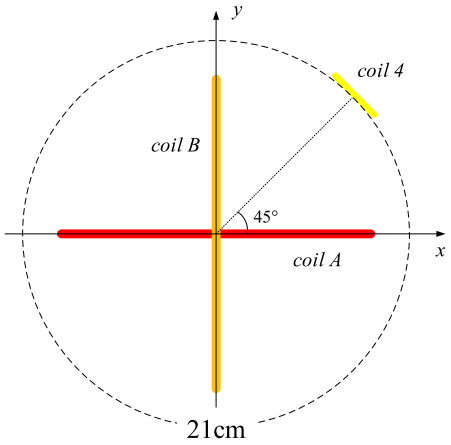

FIGURE 8. The position of receiver 4 in case I.

$$Re(Z_B) = Re(R_{xB} + \frac{L_B}{C_B(R_B + \sum_{i=1}^{n} Z_{rBi})}) = R_{xB} + \frac{L_B C_B (R_B + \sum_{i=1}^{n} \frac{\omega^2 M_{Bi}^2}{R_i + R_{Li}})}{C_B^2[(R_B + \sum_{i=1}^{n} \frac{\omega^2 M_{Bi}^2}{R_i + R_{Li}})^2 + (\sum_{i=1}^{n} \frac{\omega^2 M_{Ai} M_{Bi}}{R_i + R_{Li}})^2]} \quad (28)$$

To simplify the calculation, the parameters of two transmitters are considered as equal. $R_{xA} = R_{xB} = R_x$, $R_A = R_B = R$,$L_{xA} = L_{xB} = L_A = L_B = L$ and $C_A = C_B = C$. Based on (22-28), the transfer efficiency of load i can be expressed as (29), shown at the bottom of the next page, where,

$$\alpha_i = \frac{\omega^2 M_{Ai}^2}{R_i + R_{Li}} \quad (30)$$

$$\beta_i = \frac{\omega^2 M_{Bi}^2}{R_i + R_{Li}} \quad (31)$$

$$\gamma_i = \frac{\omega^2 M_{Ai} M_{Bi}}{R_i + R_{Li}} \quad (32)$$

$$\xi_i = \frac{R_{Li}}{R_i + R_{Li}} \quad (33)$$

From (29-33), the transfer efficiency of individual load is influenced by mutual inductance and load resistance when parameters of the transmitters are determined. Considering the parameters utilized in this paper, as shown in Table 2, the first part of denominator of η_i is much less than the second part. The transfer efficiency of load i can be simplified as (34). It is provable that η_i is positively correlated with $(M_{Ai}^2 + M_{Bi}^2)$.

$$\eta_i = \frac{(\alpha_i + \beta_i)\xi_i}{2R + \sum_{i=1}^{n} \alpha_i + \sum_{i=1}^{n} \beta_i} \quad (34)$$

2) MULTI-LOAD

With the output power and transfer efficiency of individual load obtained, the total output power P_L and transfer efficiency η of multi-load in the system can be expressed as (35-36) by summing the output power and transfer efficiency of n loads respectively.

$$P_L = \sum_{i=1}^{n} P_{Li} = \sum_{i=1}^{n} (\alpha_i + \beta_i)\xi_i \cdot I^2 \quad (35)$$

$$\eta = \sum_{i=1}^{n} \eta_i = \frac{\sum_{i=1}^{n} (\alpha_i + \beta_i)\xi_i}{2R + \sum_{i=1}^{n} \alpha_i + \sum_{i=1}^{n} \beta_i} \quad (36)$$

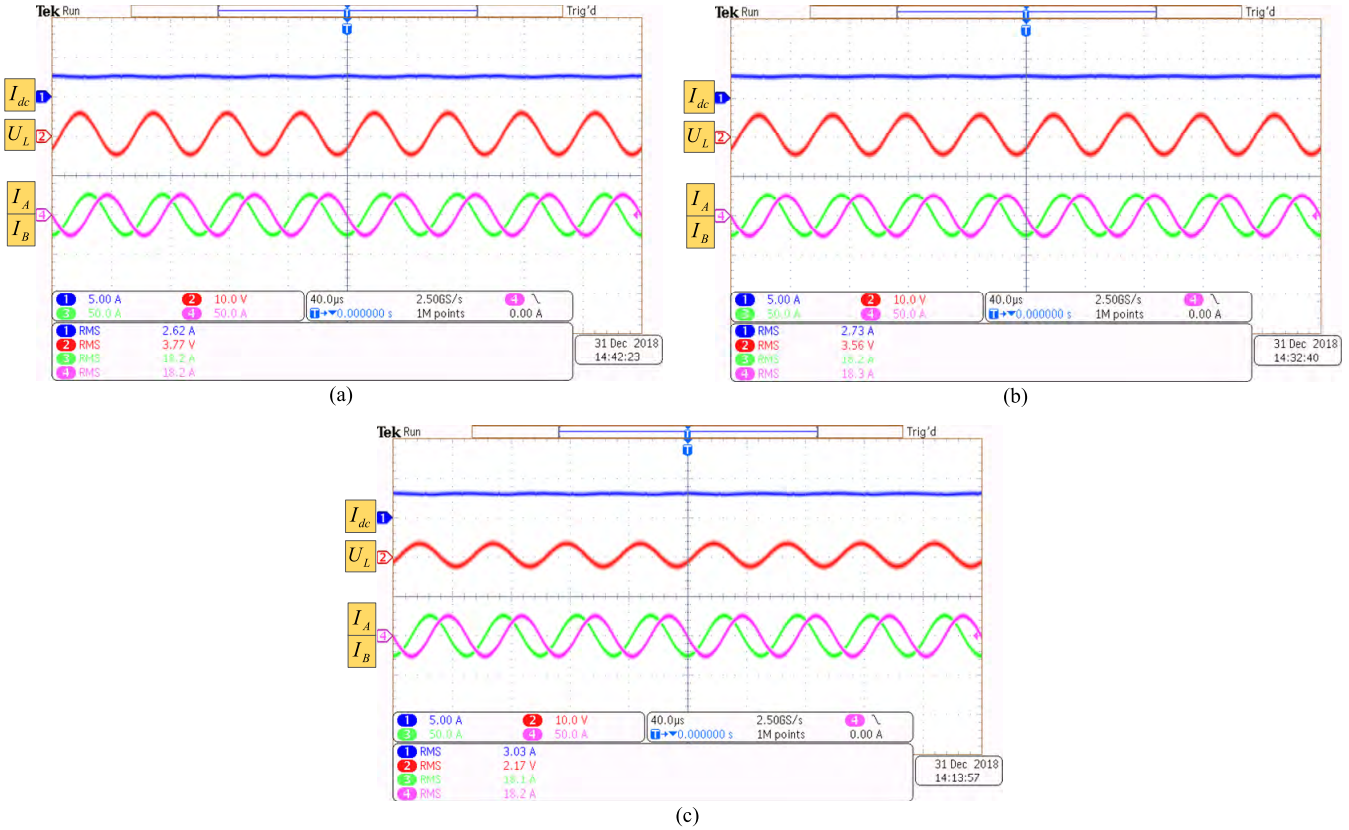

FIGURE 9. Experimental waveforms of single load with fixed position and variable resistance: (a) the resistance of load is 8Ω, (b) the resistance of load is 4Ω, and (c) the resistance of load is 0.5Ω.

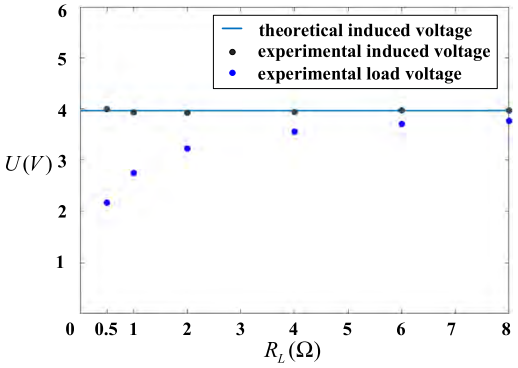

FIGURE 10. Load voltages and induced voltages under different loads.

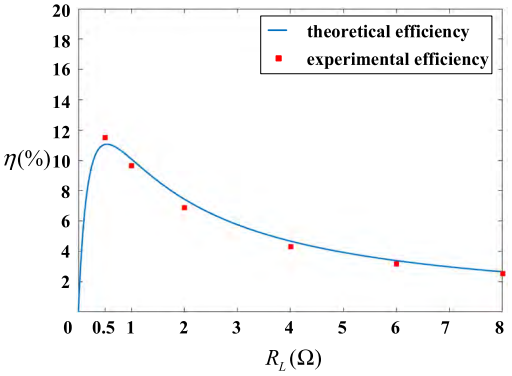

FIGURE 11. Transfer efficiency under different loads.

In practical application, compared with load resistance, the parasitic resistance is tiny which indicates $\xi_i \approx 1$ in (36). Then, (36) is derived as follows.

$$\eta = \frac{1}{\frac{2R}{\sum_{i=1}^{n}(\alpha_i+\beta_i)} + 1} \tag{37}$$

According to (5), (11), (30), (31),

$$\alpha_i + \beta_i = Z_{rAi} + Z_{rBi} \tag{38}$$

From (37-38), the total transfer efficiency is increased with the sum of impedance reflected to the two transmitters

$$\eta_i = \frac{P_{Li}}{P_A + P_B} = \frac{(\alpha_i + \beta_i)\xi_i}{\omega^2 R_x C^2[(R + \sum_{i=1}^{n}\alpha_i)^2 + (R + \sum_{i=1}^{n}\beta_i)^2 + 2(\sum_{i=1}^{n}\gamma_i)^2] + (2R + \sum_{i=1}^{n}\alpha_i + \sum_{i=1}^{n}\beta_i)} \tag{29}$$

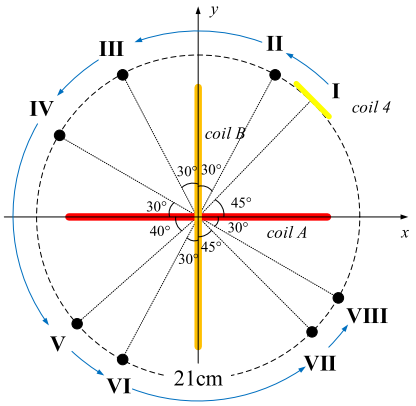

FIGURE 12. Receiver 4 moves along a circumference.

increasing, which meets the requirement of simultaneously charging multi-load.

C. UPPER LIMIT OF LOAD FOR MAINTAINING CONSTANT TRANSMITTER CURRENT

As analyzed in Section III part A, the transmitter currents are constants when the AC voltage sources and the self-inductance of the transmitter coils are determined. The derivation is on the basis of ignoring the parasitic resistors of inductors, which holds when the number and resistance of loads are not too large. In order to discuss the cases with large number of loads or heavy load, the transmitter current $\mathbf{I_A}$ is described as:

$$\mathbf{I_A} = \frac{\mathbf{U_A}}{j\omega L + j\omega C \cdot R_x(R + \sum_{i=1}^{n} Z_{rAi})} \tag{39}$$

When the proposed WPT system drives more loads or operates at heavy loads, the sum of reflected impedance $\sum_{i=1}^{n} Z_{rAi}$ in the transmitter A is larger. The second term of denominator in (39) cannot be ignored any more, and it may cause the transmitter current fluctuations. As displayed in Fig. 6, both the amplitude and the phase angle of transmitter current fluctuate. Correspondingly, the output voltage and delivered power of the receiver change.

In order to explore the maximum load capacity, a judgment rule is given in this part. As for the amplitude fluctuation, a margin λ is defined for effective value variation range. The transmitter current is considered as constant when the effective value of transmitter current varies within λ of the initial value. The amplitude constraint condition on the transmitter A is explained as:

$$||\mathbf{I_A}||_{(1)} = \frac{U_A}{\omega L} \tag{40}$$

$$||\mathbf{I_A}||_{(2)} = \frac{U_A}{\omega \sqrt{(L + CR_x(R + \sum_{i=1}^{n} \alpha_i))^2 + (CR_x(\sum_{i=1}^{n} \gamma_i))^2}} \tag{41}$$

$$||\mathbf{I_A}||_{(2)} \geq (1 - \lambda)||\mathbf{I_A}||_{(1)} \tag{42}$$

where U_A represents the effective value of AC source, $||\mathbf{I_A}||_{(1)}$ represents the initial effective value while $||\mathbf{I_A}||_{(2)}$ represents the effective value after fluctuation.

The amplitude constrain condition on the transmitter B can be derived on the same way and expressed as:

$$||\mathbf{I_B}||_{(1)} = \frac{U_B}{\omega L} \tag{43}$$

$$||\mathbf{I_B}||_{(2)} = \frac{U_B}{\omega \sqrt{(L + CR_x(R + \sum_{i=1}^{n} \beta_i))^2 + (CR_x(\sum_{i=1}^{n} \gamma_i))^2}} \tag{44}$$

$$||\mathbf{I_B}||_{(2)} \geq (1 - \lambda)||\mathbf{I_B}||_{(1)} \tag{45}$$

where U_B represents the effective value of AC source, $||\mathbf{I_B}||_{(1)}$ represents the initial effective value while $||\mathbf{I_B}||_{(2)}$ represents the effective value after fluctuation.

Based on (39), the phase angle of transmitter current A is calculated as follows,

$$\angle\theta_{iA} = \angle\theta_{uA} - \arctan \frac{L + CR_x(R + \sum_{i=1}^{n} \alpha_i)}{-CR_x \sum_{i=1}^{n} \gamma_i} \tag{46}$$

where $\angle\theta_{iA}$ and $\angle\theta_{uA}$ represent the phase angle of transmitter current $\mathbf{I_A}$ and AC source $\mathbf{U_A}$, respectively.

The phase angle of transmitter current B can be obtained on the same way, which is

$$\angle\theta_{iB} = \angle\theta_{uB} - \arctan \frac{L + CR_x(R + \sum_{i=1}^{n} \beta_i)}{CR_x \sum_{i=1}^{n} \gamma_i} \tag{47}$$

where $\angle\theta_{iB}$ and $\angle\theta_{uB}$ represent the phase angle of transmitter current $\mathbf{I_B}$ and AC source $\mathbf{U_B}$, respectively.

As evident from (46-47), when more loads are added, the phase angle change caused by recently added load is very small. Within the limitation of the transmitter current amplitudes, the current phase-shift angle of two transmitters is still around 90°, which has no effect on generating rotational magnetic field. As a result, the maximum loads capacity is depended on the amplitude constraint condition of transmitter currents.

Taking both the transmitters into consideration, the limit of the maximum load capacity of the WPT system can be

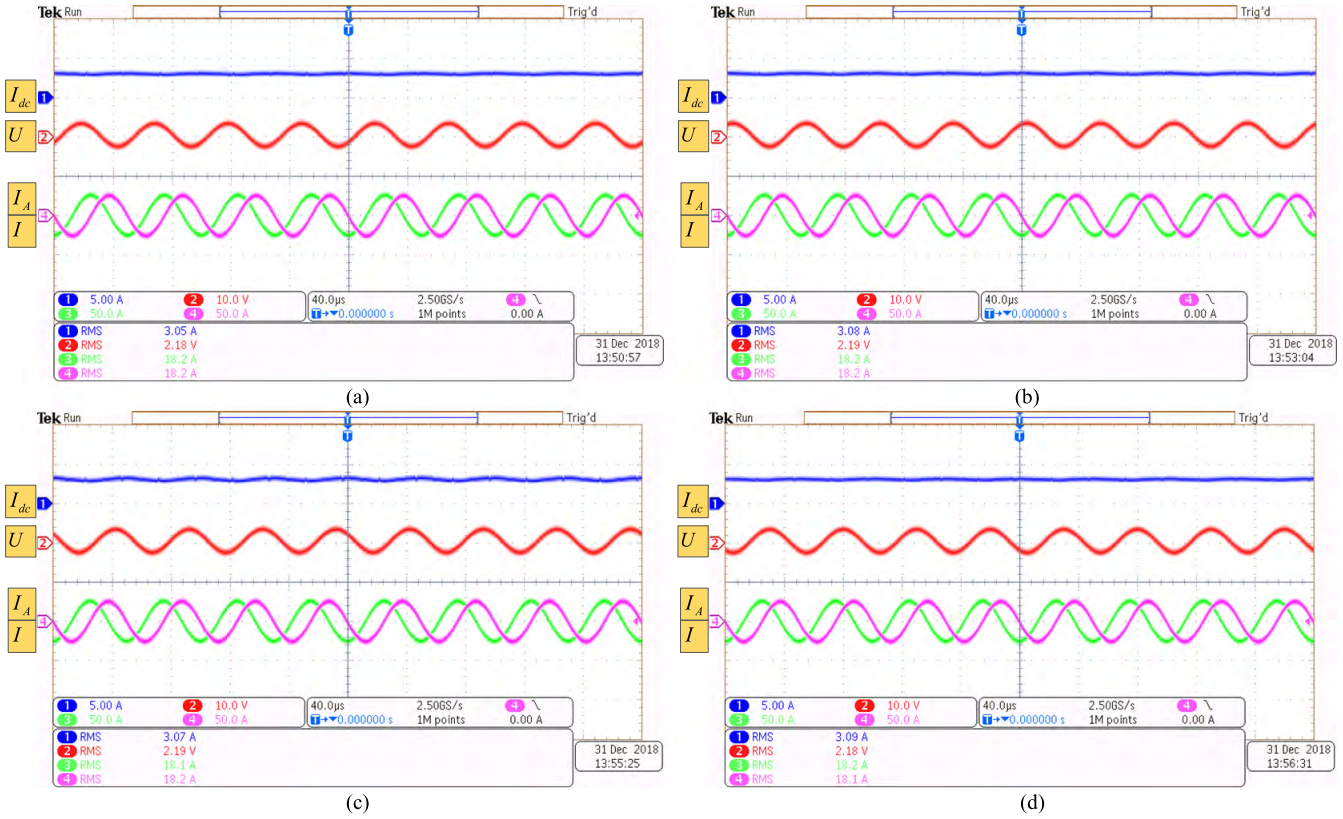

FIGURE 13. Experimental waveforms of single load placed at different locations along the same circumference: (a) the quadrant angle is 45°, (b) the quadrant angle is 120°, (c) the quadrant angle is 220°, and (d) the quadrant angle is 315°.

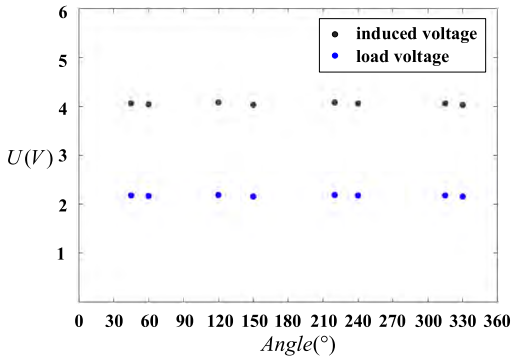

FIGURE 14. Load voltages and induced voltages at different load locations along a circumference.

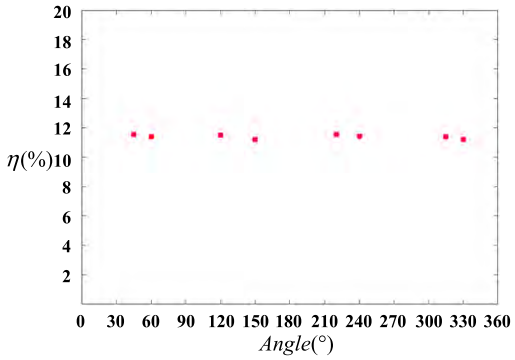

FIGURE 15. Experimental result of transfer efficiency at different load locations along a circumference.

expressed as (48).

$$\begin{cases} L^2 \geq \dfrac{(1-\lambda)^2}{2\lambda-\lambda^2}[2\omega^2 R_x(R+\sum_{i=1}^{n}\alpha_i) \\ \qquad +C^2R_x^2(R+\sum_{i=1}^{n}\alpha_i)^2+C^2R_x^2(\sum_{i=1}^{n}\gamma_i)^2] \\ L^2 \geq \dfrac{(1-\lambda)^2}{2\lambda-\lambda^2}[2\omega^2 R_x(R+\sum_{i=1}^{n}\beta_i) \\ \qquad +C^2R_x^2(R+\sum_{i=1}^{n}\beta_i)^2+C^2R_x^2(\sum_{i=1}^{n}\gamma_i)^2] \end{cases} \tag{48}$$

D. PARAMETER DESIGN GUIDANCE

The proposed 3D wireless charging cylinder is utilized for the multi-load applications, and it is significant to design proper system parameters (L, C) to meet different load requirements. Based on the system characteristics analyzed above, the system parameter designation is mainly depended on equation (48).

Considering each inductor and its corresponding capacitors resonant at operating frequency, the following condition must be satisfied.

$$2\pi \cdot f = \omega = \frac{1}{\sqrt{LC}} = \frac{1}{\sqrt{L_iC_i}} \tag{49}$$

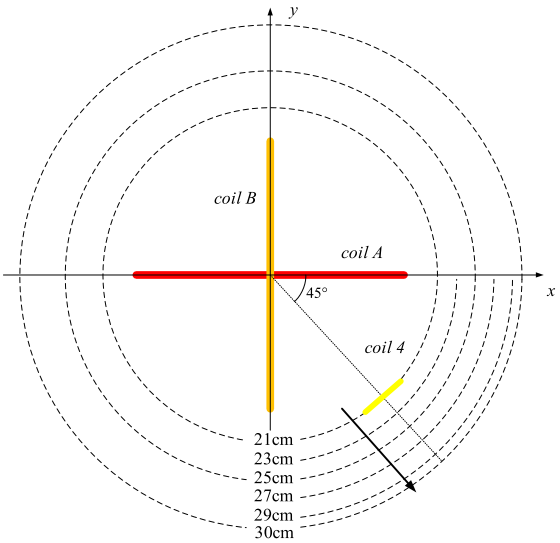

FIGURE 16. Receiver 4 placed at locations with different radial distance.

For the specific multi-load application, the load situation should be determined at first, which includes the maximum number of loads n and the variation range of load values R_{Li} during charging. Assume an extreme case that n loads are charged simultaneously and their resistance reach the minimum value $(R_{Li})_{\min}$, if (48) can be satisfied on that load situation, then the other loads situations are guaranteed to meet (48) accordingly.

Secondly, the parameters of the receiver coils should be estimated, which involves the inductance of the receiver coils L_i and its parasitic resistance R_i. Additionally, the size of receiver coils and transfer distance range also need to know, which have effects on mutual inductance M_{Ai} and M_{Bi}. The relationship between mutual inductance and self-inductance is:

$$M_{Ai} = k_{Ai}\sqrt{L \cdot L_i}, \quad M_{Bi} = k_{Bi}\sqrt{L \cdot L_i} \tag{50}$$

where k_{Ai} and k_{Bi} represent coupling coefficients of the receiver coil i and two transmitter coils. According to the analysis above, the expression of (30-32) can be transformed into (51-53).

$$\alpha_i = \frac{\omega^2 k_{Ai}^2 L L_i}{R_i + (R_{Li})_{\min}} \tag{51}$$

$$\beta_i = \frac{\omega^2 k_{Bi}^2 L L_i}{R_i + (R_{Li})_{\min}} \tag{52}$$

$$\gamma_i = \frac{\omega^2 k_{Ai} k_{Bi} L L_i}{R_i + (R_{Li})_{\min}} \tag{53}$$

Confirming the amplitude margin λ of the transmitter currents, and taking the correlation between the inductance and its corresponding parasitic resistance (L and R,

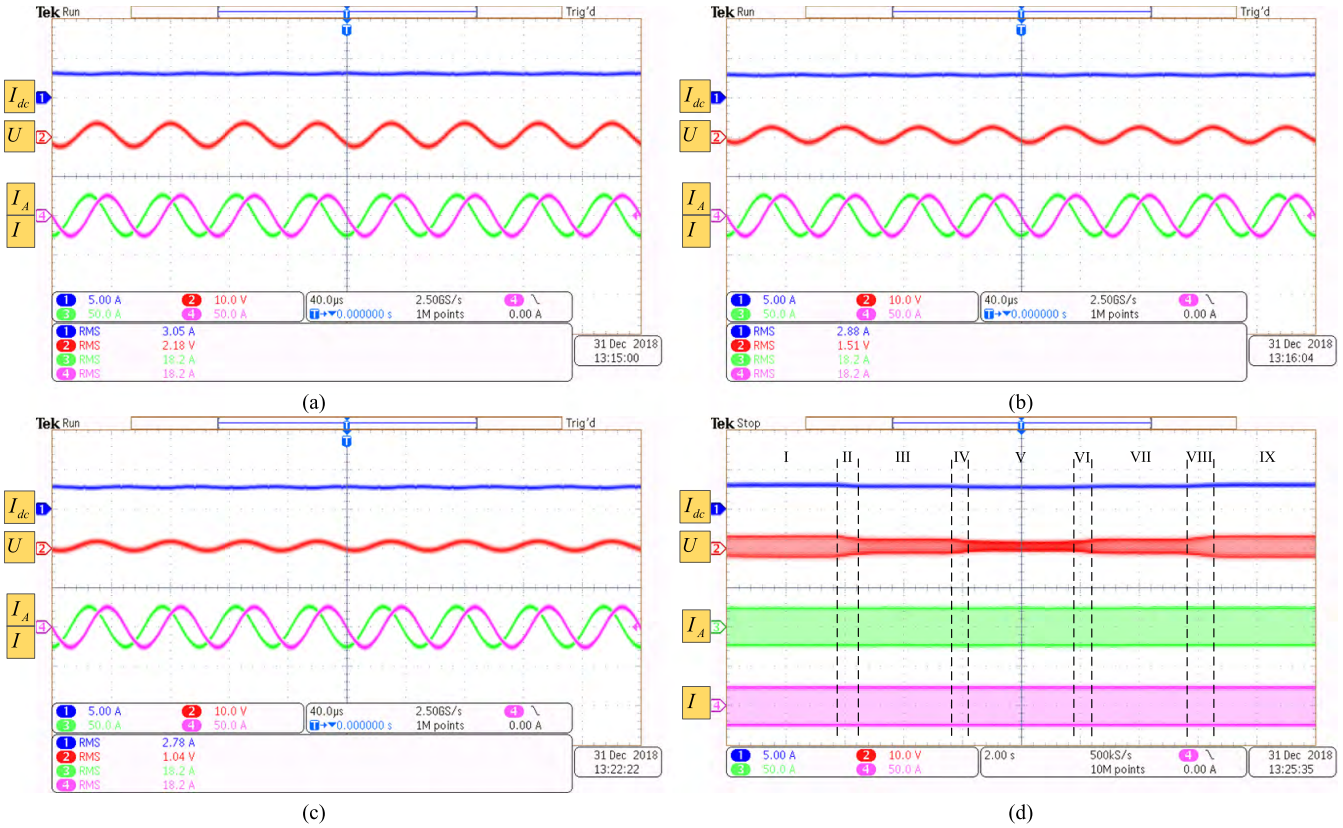

FIGURE 17. Experimental waveforms of single load placed at locations with different radial distance (a) the radial distance is 21cm, (b) the radial distance is 25cm, (c) the radial distance is 30cm, and (d) the radial distance changes as 21-25-30-25-21cm.

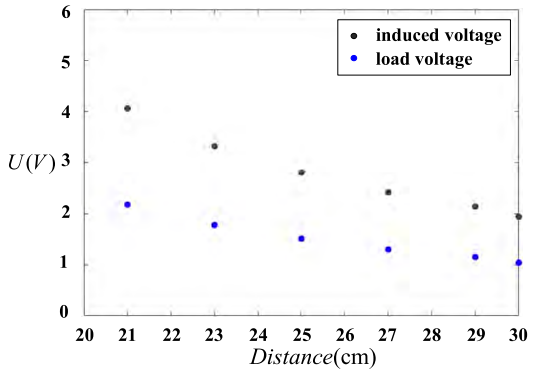

FIGURE 18. Load voltages and induced voltages at locations with different radial distance.

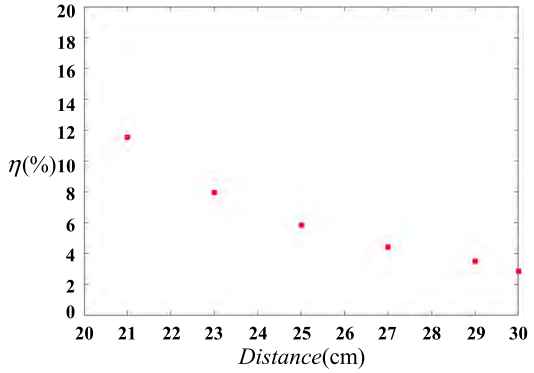

FIGURE 19. Experimental result of transfer efficiency at locations with different radial distance.

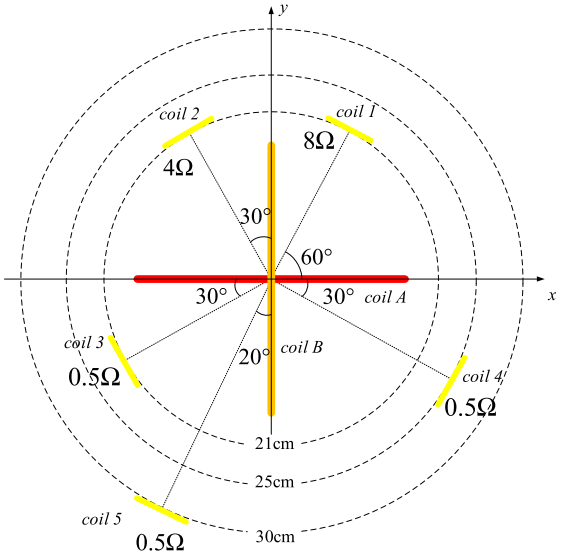

FIGURE 20. Distribution of five receivers.

L_x and R_x) into consideration, the range of the inductance L can be obtained depending on (48). Once the inductance L is determined, the other parameters of the 3D wireless charging cylinder can be determined accordingly.

IV. EXPERIMENTAL STUDY

In order to verify the above theoretical analysis, the experimental platform of the proposed 3D wireless charging cylinder is set up as shown in Fig. 7. The platform is composed of a controller equipped with a floating-point digital signal processor (DSP,TMS320F28335) and a field programmable gate array (FPGA,EP2C8J144C8N), an AC/DC converter with three independent channel 27V output, two independent controllable DC/AC converters, two LCL transmitters consisting of two inductors and a capacitor, several receiver coils connected with series resonant capacitor and resistance load. The transmitter coil is square and its side length is around 300mm. The receiver coil is circle and has a diameter of 10cm. The parameters of two transmitters and five receivers are given in Table 2 and Table 3, respectively. As explained in Section II part A, two transmitter currents are controlled to have the same amplitude and a phase difference of 90° to achieve the rotational magnetic field. The loads in the following experiments are pure resistors.

To further verify the correctness and reliability of the theoretical analysis, the experiments are carried out in three parts: single load performance evaluation, multi-load performance verification and a comparison of the proposed configuration and series-series WPT system.

TABLE 3. Actual circuit parameters of five receivers.

Description	*Parameter*	*Value*
Inductance of receiver coil 1	L_1	294 μH
Inductance of receiver coil 2, 4	L_2, L_4	297 μH
Inductance of receiver coil 3, 5	L_3, L_5	292 μH
Parasitic resistance of receiver coil 1	R_1	0.440 Ω
Parasitic resistance of receiver coil 2	R_2	0.438 Ω
Parasitic resistance of receiver coil 3	R_3	0.372 Ω
Parasitic resistance of receiver coil 4	R_4	0.432 Ω
Parasitic resistance of receiver coil 5	R_5	0.429 Ω
Resonant capacitor of receiver coil 1, 2	C_1, C_2	0.215 μF
Resonant capacitor of receiver coil 3, 5	C_3, C_5	0.216 μF
Resonant capacitor of receiver coil 4	C_4	0.213 μF
Diameter of receiver coil 1, 2, 3	d_1, d_2, d_3	98mm
Diameter of receiver coil 4, 5	d_4, d_5	97mm

A. SINGLE LOAD PERFORMANCE EVALUATION

In this part, only one load is placed in the charging area. The verification is carried out in the following three aspects to discuss the system performance. For ease of analysis, the plane of the receiver coil is perpendicular to the direction of resultant magnetic field.

1) CASE 1: SINGLE LOAD WITH FIXED POSITION AND VARIABLE RESISTANCE

This case is to simulate the load impedance variation during charging. Receiver 4 is placed at a fixed position with the radial distance of 21cm, and the offset angle relative to x-axis is 45°, as shown in Fig. 8. The resistances of loads are selected as 8Ω, 6Ω, 4Ω, 2Ω, 1Ω and 0.5Ω.

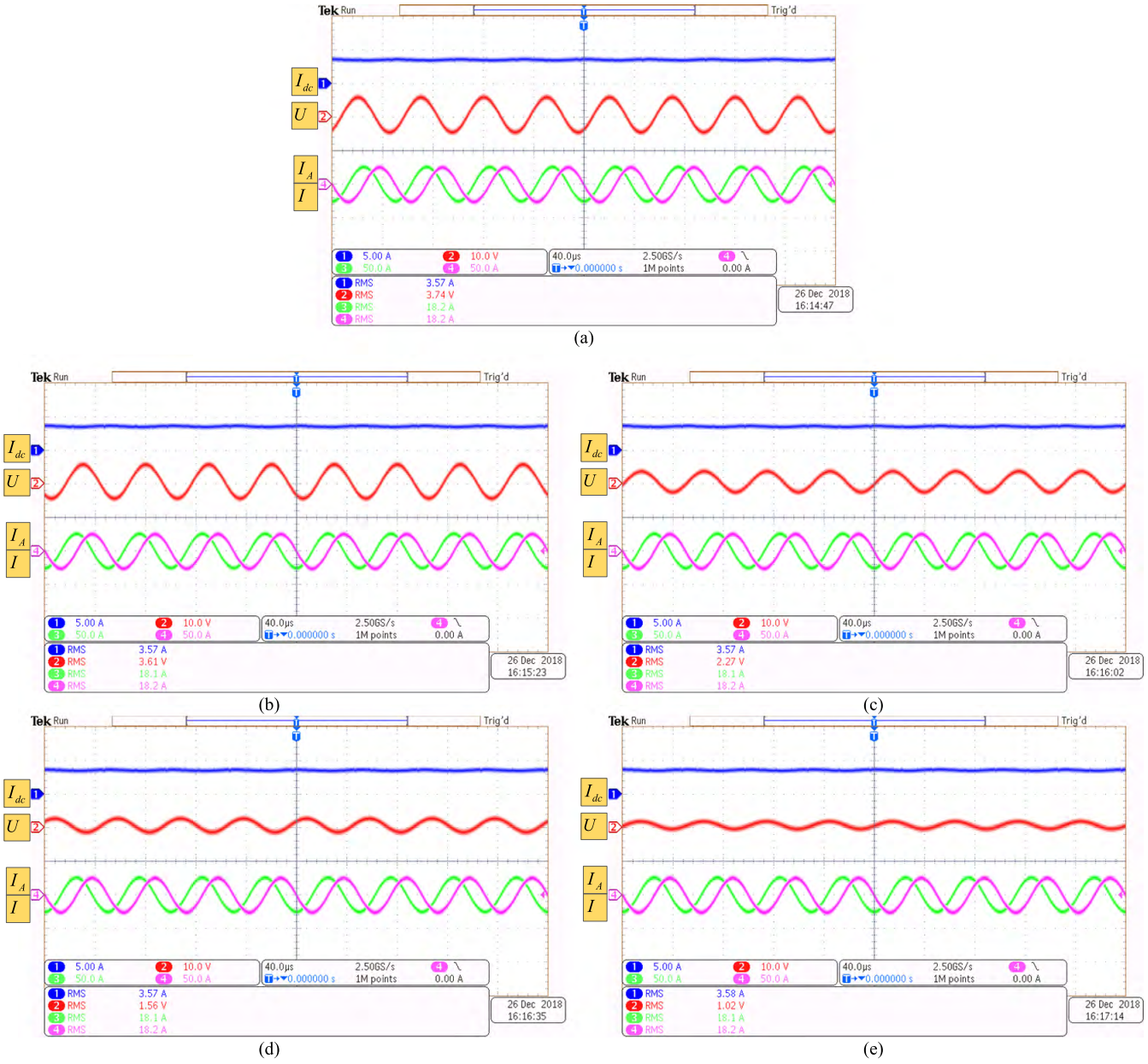

FIGURE 21. Experimental waveforms of multi-load placed at different locations: (a) load 1 with resistance of 8Ω and radial distance of 21cm, (b) load 2 with resistance of 4Ω and radial distance of 21cm, (c) load 3 with resistance of 0.5Ω and radial distance of 21cm, (d) load 4 with resistance of 0.5Ω and radial distance of 25cm, and (e) load 5 with resistance of 0.5Ω and radial distance of 30cm.

Fig. 9 shows the waveforms when the resistances of load are 8Ω, 4Ω, 0.5Ω. The waveforms from top to bottom in the following figures are input DC current I_{dc}, load voltage U_L and two transmitter currents I_A and I_B, and this order is also applicable to the other waveforms in the rest of this paper. As can be seen from Fig. 9 (a-c), the change in load resistance has no effect on the transmitter currents. The two transmitter currents are stable at around 18.2A and the phase-shift angle between them is 90°. When the resistance of load changes from 8Ω to 0.5Ω, the load resistance gradually approaches the parasitic resistance of receiver coil 4. As a result, the load voltage changes from 3.77V to 2.17V. The induced voltages of different loads can be calculated according to (18) and they are displayed in Fig. 10. The induced voltages are approximately at 4V and unaffected by load resistance change. On the basis of the experimental measurements, the transfer efficiency at different loads are drawn in Fig. 11. The power loss on two inverters are theoretically considered as constant since the currents flowing through them are essentially unchanged when the load resistance changes. Obviously, the experimental result of transfer efficiency increases with the load resistance decreasing, which is consistent with the theoretical results. When $R_L = 0.5\Omega$, the load power and experimental transfer efficiency are 9.42W and 11.5%.

2) CASE 2: SINGLE LOAD PLACED AT DIFFERENT LOCATIONS ALONG THE SAME CIRCUMFERENCE

As shown in Fig. 12, the receiver 4 moves along the circumference with a radius of 21cm. Eight locations on the circumference are chosen randomly. They are distributed in four quadrant with the quadrant angles are 45°, 60°, 120°, 150°, 220°, 240°, 315°, 330°, respectively. Receiver 4 is first placed at location I with the quadrant angle of 45° and then successively placed at the other seven locations in a counterclockwise direction. The resistance of load is selected as 0.5Ω.

Fig. 13 shows the waveforms when receiver 4 is placed at the locations with quadrant angle of 45°, 120°, 220°, 315°, respectively. As can be seen from Fig. 13 (a-d), when load moves along the circumference, two transmitter currents are stable at around 18.2A and the phase-shift angle between them is 90°. The effective value of load voltage is maintained around 2.18V. The induced voltages and transfer efficiency at different locations along the circumference can be calculated, as shown in Fig. 14 and Fig. 15. The induced voltage and transfer efficiency are kept at around 4V and 11.5%, which are unaffected when load location changes along a circumference.

3) CASE 3: SINGLE LOAD PLACED AT LOCATIONS WITH DIFFERENT RADIAL DISTANCE

In this case, the load resistance is 0.5Ω. The receiver 4 is first placed at the location with radial distance of 21cm and the offset angle relative to x-axis is 315°. Then the receiver 4 is successively placed at locations in the same direction with the radial distance of 23cm, 25cm, 27cm, 29cm, 30cm, respectively, as shown in Fig. 16.

Fig. 17 shows the waveforms when the radial distance is 21cm, 25cm, 30cm, respectively. It is evident from Fig. 17 (a-c) that the transmitter currents are unaffected by the distance from the transmitter center to the receiver center changing. The effective values of transmitter currents are maintained at around 18.2A and the phase-shift angle between them is 90°. According to the information obtained from measurements, the induced voltage and the transfer efficiency can be calculated, as shown in Fig. 18 and Fig. 19, respectively. The induced voltage changes from 4V to 2V and the transfer efficiency changes from 11.5% to 2.9%, both of which decrease with the radial distance increasing. Fig. 17 (d) displays the complete process when the radial distance varies from 21cm to 30cm and then returns to 21cm. Process I, III, V, VII, IX represent the radial distance of 21cm, 25cm, 30cm, 25cm, 30cm, respectively. The other processes represent the dynamic change of radial distance. The waveforms variation in Fig. 17 (d) are completely consistent with the analysis above.

B. B.MULTI-LOAD PERFORMANCE VERIFICATION

To simulate the practical application of charging multi-load simultaneously, five receivers are placed randomly in the charging area in this experiment. As displayed in Fig. 20, three receivers are placed at the circumference with the radius of 21cm, and their quadrant angles are 60°, 120°, 210°, respectively. The other two receivers are placed at locations with the radial distance of 25cm and 30cm, and their quadrant angles are 330° and 250°. The resistances of five loads are selected as 8Ω, 4Ω, 0.5Ω, 0.5Ω, 0.5Ω.

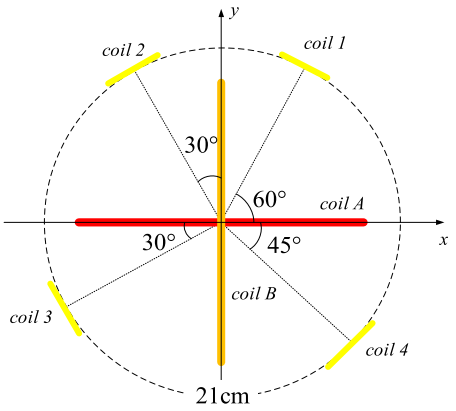

FIGURE 22. Distribution of four receivers.

TABLE 4. Induced voltages of five loads.

Description	*Load 1*	*Load 2*	*Load 3*	*Load 4*	*Load 5*
Resistance (Ω)	8	4	0.5	0.5	0.5
Radial distance (cm)	21	21	21	25	30
Load voltage (V)	3.74	3.61	2.27	1.56	1.02
Inducted voltage (V)	3.95	4.01	3.96	2.91	1.90

The waveforms of five loads are presented in Fig. 21. The effective values of transmitter currents are all stable at around 18.2A and the phase-shift angle between them is 90°, which remain constant against load variations. According to (18) and the circuit parameters given in Table 3, the induced voltages of five loads can be calculated, as shown in Table 4. Load 1-3 have the same radial distance and different resistance, the induced voltages of which are around 4V and unaffected by resistance changing. Load 3-5 have the same resistance and different radial distance, the induced voltages of which decrease with the radial distance increasing. The voltage characteristics of multi-load system are consistent with the single load system analyzed in Part A. Compare Fig. 21 (a-c) with Fig. 9 (a-c), Fig. 21 (d-e) with Fig. 17 (b-c), respectively, the voltage of each load in the multi-load system is the same as in the single load system, which is not influenced by the other load joins. Based on the measurements in this experiment, it can be calculated that the total output power is 22.3W and the transfer efficiency of this multi-load system is 23.1%.

C. COMPARISON BETWEEN THE PROPOSED CONFIGURATION AND CONVENTIONAL SS COMPENSATED WPT SYSTEM

This experiment is set to compare the performance of the proposed configuration with the conventional SS compensated

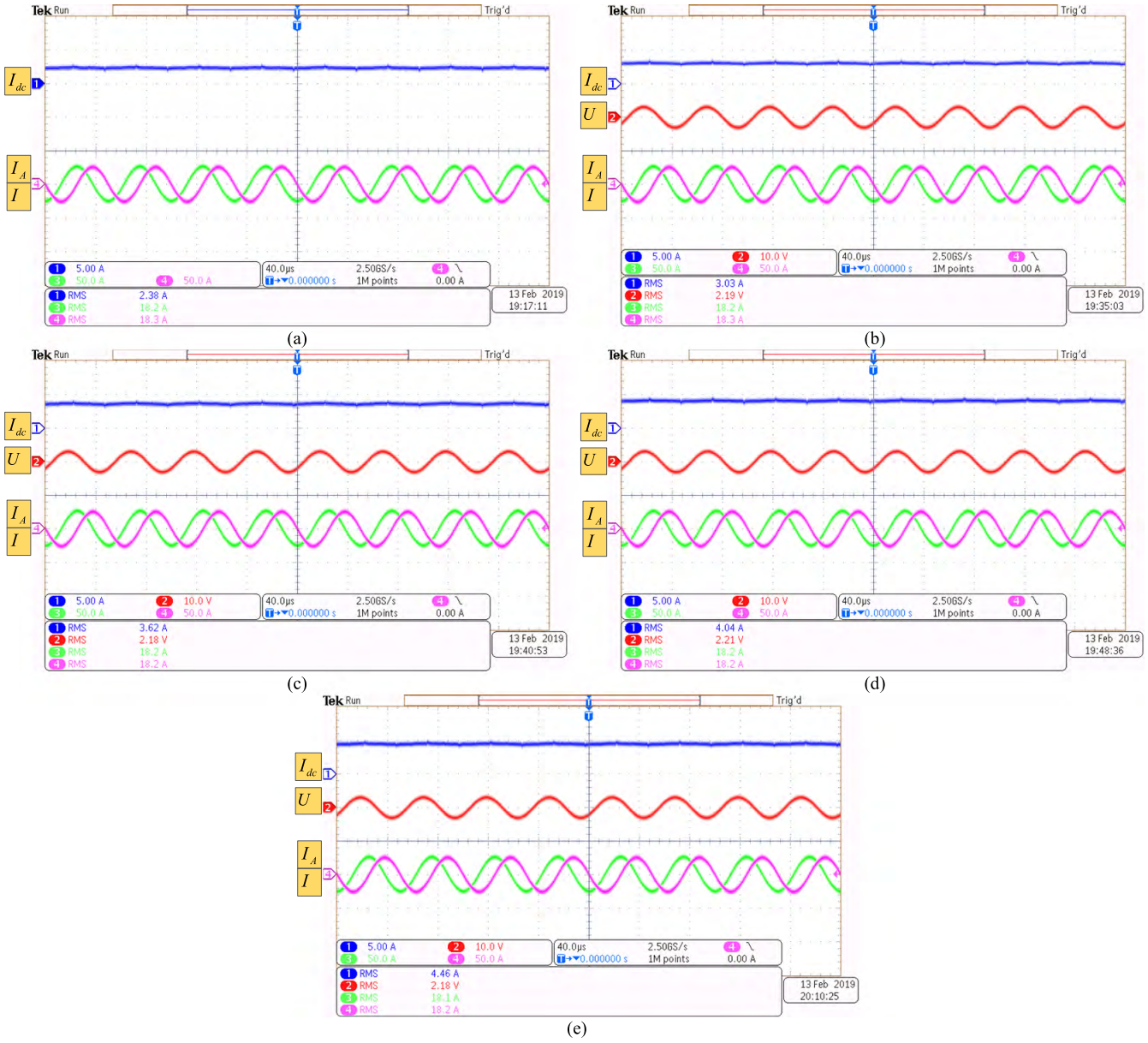

FIGURE 23. Experimental waveforms under different load situations in the proposed configuration (a) under no load, (b) when only receiver 1 is placed, (c) when receiver 2 is placed, (d) when receiver 3 is placed, and (e) when receiver 4 is placed.

TABLE 5. Voltages of four loads under proposed and conventional systems.

System Type	U_{L1}	U_{L2}	U_{L3}	U_{L4}
Proposed System	2.18V	2.10V	2.13V	2.18V
Conventional System	1.88V	1.98V	1.85V	1.86V

WPT system. As shown in Fig. 22, four receivers are distributed in four quadrants with the quadrant angles of 60°, 120°, 210°, 315°, respectively. To clearly observe the change of waveforms of loads, four receivers are placed along the same circumference with the radial distance of 21cm, and the resistance of four loads are selected as 0.5Ω.

Fig. 23 shows the experimental results when receiver 1-4 are successively placed in the charging area of the proposed configuration. Fig. 23 (a) shows the waveforms under no load and Fig. 23 (b) shows the waveforms when only load 1 is placed. Fig. 23 (c-e) show the waveforms for recently added loads, respectively. In order to observe the effect of the load added later on the load already added, the voltage of load 1 under different load situations is recorded, as shown in the second channel of the waveforms in Fig. 23 (b-e). As can be seen from Fig. 23, the transmitter currents are kept constant against load variation and the voltage of load 1 is unaffected by the other loads added later. Table 5 lists the voltages of four loads when all of them are placed. It can be calculated that the total output power reaches 36.9W and the transfer efficiency is 30.6%. The transfer efficiency in this case is higher than

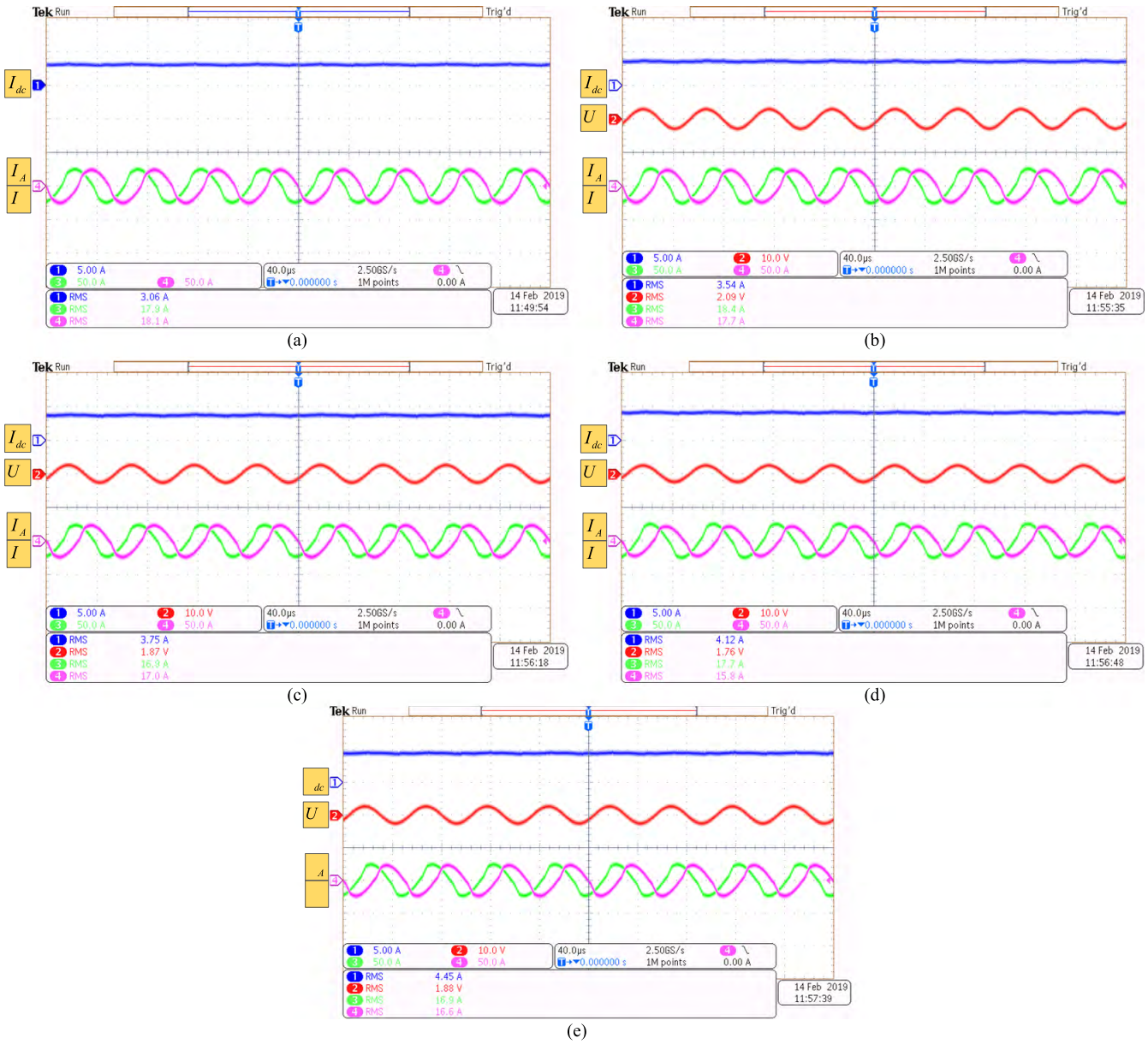

FIGURE 24. Experimental waveforms under different load situations in the SS compensated WPT system (a) under no load, (b) when only receiver 1 is placed, (c) when receiver 2 is placed, (d) when receiver 3 is placed, and (e) when receiver 4 is placed.

that of the experiment in part B because of the larger total reflected impedance to the transmitters.

The experimental results of the SS compensated system under the same conditions are displayed in Fig. 24. Fig. 24 (a) shows the waveforms under no load, two transmitter currents are adjusted to around 18A at first to generate the same magnitude rotating magnetic field as the proposed configuration. Then the four receivers are placed at the same locations successively as the last experiment. Fig. 24 (b) shows the waveforms when only load 1 is placed. Fig. 24 (c-e) show the waveforms for recently added loads, respectively. The second channel of the waveforms in Fig. 24 (b-e) represents the voltage of load 1. It is obvious that the two transmitter currents vary with recently added loads and drop to around 16.6A when four loads are placed. From Fig. 24 (b) to Fig. 24 (e), the voltage of load 1 is affected by the subsequently added loads and changes from 2.09V to 1.88V. When the last load is added, the voltages of four loads are listed in Table 5. It can be obtained that the total output power is 28.7W and the transfer efficiency is 23.7%.

Based on the experimental results obtained above, the rotating magnetic field generated by the proposed configuration is more stable than that of the SS compensated system, which mainly reflect on the following aspects: 1) the proposed configuration can maintain the transmitter current to be constant within the maximum load limit; 2) multiple loads can be added without affecting each other in the proposed configuration.

V. CONCLUSION

This paper proposes a 3D wireless charging cylinder for the multi-load application, which generates stable rotating magnetic field. The transmitter currents remain constant against load variations when the total load is within the maximum load limit. The inducted voltage of each receiver only depends on the distance between the transmitter and the receiver, and the transfer efficiency increases with the total reflected impedance increasing. The experimental results verified the effectiveness of the proposed system. Compared to the conventional SS compensated WPT system, the proposed 3D configuration can maintain the transmitter current to be constant within the maximum load limit so that multiple loads can be added without affecting each other, which indicates the proposed configuration generates a more stable rotating magnetic field and is more suitable for multi-load application.

REFERENCES

[1] W. Zhang *et al.*, "High-efficiency wireless power transfer system for 3D, unstationary free-positioning and multi-object charging," *IET Electr. Power Appl.*, vol. 12, no. 5, pp. 658–665, Apr. 2018. doi: 10.1049/iet-epa.2017.0581.

[2] H. H. Lee, S. H. Kang, and C. W. Jung, "MR-WPT with reconfigurable resonator and ground for laptop application," *IEEE Microw. Wireless Compon. Lett.*, vol. 28, no. 3, pp. 269–271, Mar. 2018. doi: 10.1109/LMWC.2018.2802719.

[3] S. H. Kang, V. T. Nguyen, and C. W. Jung, "Analysis of MR-WPT using planar textile resonators for wearable applications," *IET Microw., Antennas Propag.*, vol. 10, no. 14, pp. 1541–1546, Nov. 2016. doi: 10.1049/iet-map.2016.0024.

[4] L. Li, H. Liu, H. Zhang, and W. Xue, "Efficient wireless power transfer system integrating with metasurface for biological applications," *IEEE Trans. Ind. Electron.*, vol. 65, no. 4, pp. 3230–3239, Apr. 2018. doi: 10.1109/TIE.2017.2756580.

[5] B. Lee, M. Kiani, and M. Ghovanloo, "A triple-loop inductive power transmission system for biomedical applications," *IEEE Trans. Biomed. Circuits Syst.*, vol. 10, no. 1, pp. 138–148, Feb. 2016. doi: 10.1109/TBCAS.2014.2376965.

[6] A. A. S. Mohamed, A. Berzoy, and O. A. Mohammed, "Experimental validation of comprehensive steady-state analytical model of bidirectional WPT system in EVs applications," *IEEE Trans. Veh. Technol.*, vol. 66, no. 7, pp. 5584–5594, Jul. 2017. doi: 10.1109/TVT.2016.2634159.

[7] R. Mai, Y. Chen, Y. Zhang, N. Yang, G. Cao, and Z. He, "Optimization of the passive components for an S-LCC topology-based WPT system for charging massive electric bicycles," *IEEE Trans. Ind. Electron.*, vol. 65, no. 7, pp. 5497–5508, Jul. 2018. doi: 10.1109/TIE.2017.2779437.

[8] S. Huang, Z. Li, Y. Li, X. Yuan, and S. Cheng, "A comparative study between novel and conventional four-resonator coil structures in wireless power transfer," *IEEE Trans. Magn.*, vol. 50, no. 11, Nov. 2014, Art no. 8401704. doi: 10.1109/TMAG.2014.2331962.

[9] J. Zhang, X. Yuan, C. Wang, and Y. He, "Comparative analysis of two-coil and three-coil structures for wireless power transfer," *IEEE Trans. Power Electron.*, vol. 32, no. 1, pp. 341–352, Jan. 2017. doi: 10.1109/TPEL.2016.2526780.

[10] J. Zhao, T. Cai, S. Duan, H. Feng, C. Chen, and X. Zhang, "A general design method of primary compensation network for dynamic WPT system maintaining stable transmission power," *IEEE Trans. Power Electron.*, vol. 31, no. 12, pp. 8343–8358, Dec. 2016. doi: 10.1109/TPEL.2016.2516023.

[11] Y. Yao, Y. Wang, X. Liu, F. Lin, and D. Xu, "A novel parameter tuning method for a double-sided *LCL* compensated WPT system with better comprehensive performance," *IEEE Trans. Power Electron.*, vol. 33, no. 10, pp. 8525–8536, Oct. 2018. doi: 10.1109/TPEL.2017.2778255.

[12] A. Kurs, A. Karalis, J. D. Joannopoulos, and M. Soljacic, "Wireless power transfer via strongly coupled magnetic resonance," *Science*, vol. 317, no. 5834, pp. 83–86, Jul. 2007. doi: 10.1126/science,1143254.

[13] D. Zhigang, C. Yuan, and J. A. Abu Qahouq, "Reconfigurable magnetic resonance-coupled wireless power transfer system," *IEEE Trans. Power Electron.*, vol. 30, no. 11, pp. 6057–6069, Nov. 2015. doi: 10.1109/TPEL.2015.2422776.

[14] D. Ahn and S. Hong, "A study on magnetic field repeater in wireless power transfer," *IEEE Trans. Ind. Electron.*, vol. 60, no. 1, pp. 360–371, Jan. 2013. doi: 10.1109/TIE.2012.2188254.

[15] P. K. S. Jayathurathnage, A. Alphones, and D. M. Vilathgamuwa, "Optimization of a wireless power transfer system with a repeater against load variations," *IEEE Trans. Ind. Electron.*, vol. 64, no. 10, pp. 7800–7809, Oct. 2017. doi: 10.1109/TIE.2017.2696499.

[16] K. O'Brien, "Inductively coupled radio frequency power transmission system for wireless systems," Ph.D. dissertation, Dept. Elect. Eng., Techn. Univ. Dresden, Dresden, Germany, pp. 47–62.

[17] D. Lin *et al.*, "Mathematical analysis of omnidirectional wireless power transfer—Part-I: Two-dimensional systems," *IEEE Trans. Power Electron.*, vol. 32, no. 1, pp. 625–633, Jan. 2017. doi: 10.1109/TPEL.2016.2523500.

[18] Y. Lim *et al.*, "A novel phase-control-based energy beamforming techniques in nonradiative wireless power transfer," *IEEE Trans. Power Electron.*, vol. 30, no. 11, pp. 6274–6287, Nov. 2015. doi: 10.1109/TPEL.2014.2379672.

[19] Q. Zhu *et al.*, "Field orientation based on current amplitude and phase angle control for wireless power transfer," *IEEE Trans. Ind. Electron.*, vol. 65, no. 6, pp. 4758–4770, Jun. 2018. doi: 10.1109/TIE.2017.2767556.

[20] T. Mei *et al.*, "Magnetic-field-model based analysis of two-phase magnetically coupled resonant wireless power transfer system," in *Proc. IEEE Appl. Power Electron. Conf. Expo. (APEC)*, San Antonio, TX, USA, Mar. 2018, pp. 1092–1097. doi: 10.1109/APEC.2018.8341152.

[21] P. Raval *et al.*, "Multiphase inductive power transfer box based on a rotating magnetic field," *IEEE Trans. Ind. Electron.*, vol. 62, no. 2, pp. 795–802, Feb. 2015. doi: 10.1109/TIE.2014.2334666.

HUA HAN was born in Hunan, China, in 1970. She received the M.S. and Ph.D. degrees from the School of Automation, Central South University, Changsha, China, in 1998 and 2008, respectively. She was a Visiting Scholar with the University of Central Florida, Orlando, FL, USA, from 2011 to 2012. She is currently a Professor with the School of Automation, Central South University. Her research interests include microgrids, renewable energy power generation systems, and power electronic equipment.

ZHU MAO was born in Hubei, China, in 1995. She received the B.S. degree in electrical engineering and automation from Central South University, Changsha, China, in 2016, where she is currently pursuing the M.S. degree in electrical engineering. Her research interest includes wireless power transfer.

QI ZHU was born in Anhui, China, in 1993. He received the B.S. degree in electrical engineering and automation from Central South University, Changsha, China, in 2014, where he is currently pursuing the Ph.D. degree in electrical engineering. Since 2017, he has been a joint Ph.D. student funded by the China Scholarship Council at The University of Auckland, Auckland, New Zealand. His research interests include wireless power transfer and matrix converters.

MEI SU was born in Hunan, China, in 1967. She received the B.S. degree in automation and the M.S. and Ph.D. degrees in electric engineering from the School of Automation, Central South University, in 1989, 1992, and 2005, respectively, where she has been a Professor with the School of Automation, since 2006. Her research interests include matrix converters, adjustable speed drives, and wind energy conversion systems.

AIGUO PATRICK HU received the B.E. and M.E. degrees from Xian Jiaotong University, Xi'an, China, in 1985 and 1988, respectively, and the Ph.D. degree from The University of Auckland, Auckland, New Zealand, in 2001. He was a Lecturer and the Director of the China Italy Cooperative Technical Training Center, Xi'an, and the General Manager of a technical development company. Funded by the Asian2000 Foundation, he was with the National University of Singapore for a semester as an Exchange Postdoctoral Research Fellow. He is currently with the Department of Electrical and Computer Engineering, The University of Auckland, and also the Head of Research of PowerbyProxi, Ltd. He holds 15 patents in wireless/contactless power transfer and microcomputer control technologies, and has published more than 200 peer-reviewed journal and conference papers, authored a monograph on wireless inductive power transfer technology, and contributed four book chapters.